



# Evaluation of PWV products derived from satellite-based and radiosonde retrievals for the eastern anatolia observatory (DAG)

Recep Balbay<sup>1,2</sup> · Kazım Kaba<sup>2</sup> · Süleyman Fişek<sup>3,4</sup> · Cahit Yeşilyaprak<sup>2,4</sup>

Received: 25 January 2024 / Accepted: 21 July 2024 / Published online: 29 July 2024  
© The Author(s) 2024

## Abstract

In this study, we have presented the results of the precipitable water vapor (PWV) for the Eastern Anatolia Observatory (in Turkish: Doğu Anadolu Gözlemevi, the acronym is DAG) site in Erzurum, Türkiye. The DAG has Türkiye's largest and the first near infrared (NIR) telescope with a mirror diameter of 4 meters at the altitude of 3170 m. The DAG telescope is going to take the first light in the end of summer 2024. This study is focused on the examining of the precipitable water vapor data for the NIR observations at the DAG. In this context, the NWC SAF Total Precipitable Water (TPW) data obtained by both the satellite based and the radiosonde balloon validated with six radiosonde stations were examined by temporal, vertical and horizontal analyses for the DAG site between June 2019 to December 2020. The results obtained from these analyzes indicate that the mean and median TPW values at the DAG site were approximately 7 mm and the minimum and maximum values were 0.59 mm and 24.12 mm, respectively. The monthly median TPW values at the DAG site varied between approximately 3-10 mm, with a decreasing trend from June to January and an increase in the first seven months of 2020. These results also indicate that the TPW data obtained by its 15 minutes temporal resolution, aligns closely with the radiosonde measurements. Furthermore, the values of PWV at both lower and upper levels of the atmosphere are minimal while the values increase slightly in the middle layer of the atmosphere. As a result, the effective monitoring of the PWV in a site would result in the generation of higher quality astronomical IR observations and be important in terms of the optimum operating cost for an observatory.

**Keywords** Precipitable water vapor · Astronomy · Remote sensing · Eastern anatolia observatory (DAG)

## 1 Introduction

The atmosphere of Earth significantly limits astronomical observations beyond the role in sustaining life. The Earth's atmosphere contains a mixture of several gases, such

---

Extended author information available on the last page of the article

as  $N_2$ ,  $O_2$ , Ar,  $CO_2$ ,  $O_3$ , etc. and these gases significantly influence the atmospheric absorption characteristics [1]. The water vapor in the atmosphere also contributes to opacity in the infrared spectrum, particularly at mid-infrared and far-infrared wavelengths [2]. Consequently, the monitoring of precipitable water vapor (PWV) along the atmospheric column over multiple years is crucial to identifying optimal sites to establish an observatory which will make observation in microwave, millimeter, sub-millimeter and infrared regions. The impact of water vapor is prominently observed in the near infrared spectral range, specifically at wavelengths below 3000 nanometers. Figure 1 shows a simulated Earth transmission spectrum generated using the NASA Planetary Spectrum Generator (PSG) tool [3].

Some factors as astronomical seeing, cloud cover, humidity, wind and water vapor are the decision maker for the site selection for an observatory. Therefore, PWV is also a crucial atmospheric component for infrared (IR) observations [4] and affects the accuracy and reliability of these observations through its absorption and re-emission of infrared radiation. Moreover, the level of atmospheric water vapor is pivotal in shaping the accuracy and quality of infrared (IR) observations [5].

The PWV measured in millimeters or centimeters quantifies the total water vapor from the surface of the Earth to the upper atmosphere, representing the depth of water in a vertical column of unit cross-sectional area if liquefied [6]. The PWV introduces phase errors, excess noise, and coherence loss, which affect the precision of infrared observations [7]. It should be recognized that PWV is influenced both by altitude and geographical latitude [8]. However, water vapor is the main greenhouse gas responsible for the most significant absorption compared to other gases [9]. Additionally, the re-emission of absorbed energy contributes to the sky background, impacting the sensitivity of IR observations [10].

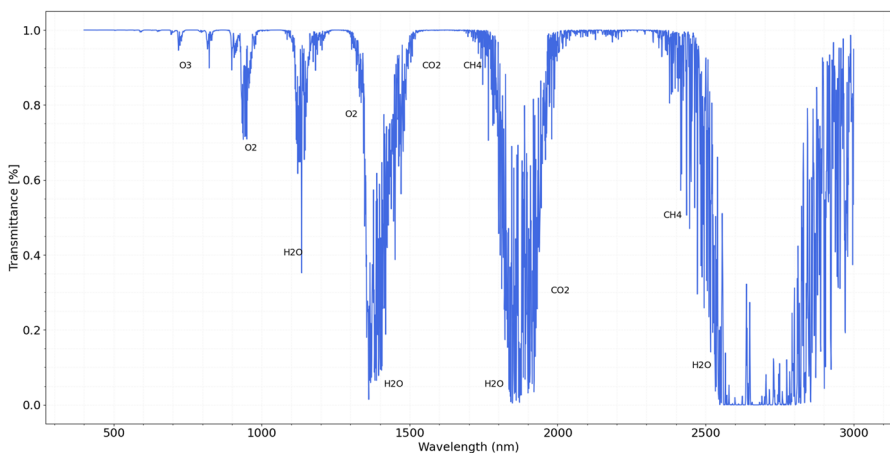


**Fig. 1** Atmospheric transmittance due to gases absorption as a function of wavelength. The Earth's transmission spectra (from 400nm to 3000nm) were generated using the NASA Planetary Spectrum Generator (PSG) tool. Atmosphere and surface composition as follows surface pressure:  $5.8546e-01$  bar; Molecular weight: 28.97 g/mol; Gases:  $H_2O$ ; Surface temperature: 275.45K; Albedo: 0.30; Emissivity:0.70

Evaluating atmospheric properties through on-site ground-based meteorological data and formulating extensive observational strategies is essential, but may not be sufficient. Numerous site evaluation studies have been carried out to identify suitable locations for astronomy worldwide [11]. Research on PWV monitoring for both potential and active observatory sites globally, including high altitude sites in Chile [12, 13], Kitt Peak National Observatory (KPNO) [14], Roque de los Muchachos Observatory (ORM) [15], and the Thirty Meter Telescope (TMT) [16], is being conducted.

Astronomical observatories are ideally located at a top of high mountains to circumvent the adverse impacts of the Earth's atmosphere, including atmospheric turbulence, attenuation, scattering, and spectral absorption lines. The DAG (with its new administrative structure and name Türkiye National Observatories) is located at an altitude of 3170 m, which is the highest altitude and the robust infrastructure observatory site in Türkiye, and is planned to serve as an observatory around the world [17]. The aim of this study is to examine the precipitable water vapor for the NIR observations at the DAG and to make higher quality NIR observations.

## 2 Study area and data

Today, it has become quite common to see the use of various techniques (satellite-based, ground-based, such as GPS meteorology or radiosonde balloons) for different purposes in many different disciplines [18–21]. The objective of this research is to create a database of PWV data gathered through various methods such as satellite imagery and a radiosonde balloon, with the purpose of comparing these data sets and conducting temporal analyzes.

The DAG site as Türkiye's the largest observatory site was selected as the locations for this study. First of all, the TPW values from the satellite were compared with the PWV values from radiosonde stations distributed homogeneously throughout Türkiye. The analyses of PWV values from satellite for the DAG site were made using the NWC SAF SPhR product. The PWV data from radiosonde observations for the DAG were also supplied by the Türkiye State Meteorological Service (TSMS). Both limitations in temporal resolution (with observations conducted only at 00:00 UTC and 12:00 UTC, daily) and the atmospheric drift effect of the balloon data from Erzurum meteorological ground station (17095-ERZM), where far away about 14 km, were taken into consideration for the PWV analyses for the DAG site. After the radiosonde balloon launch, it may deviate easily from their initial launch point due to wind or turbulence. These deviations take place typically within a few kilometers in the lower troposphere and also increase with altitude. These drift variations are highly influenced by the seasonal weather conditions of the location [22].

As the preliminary information, it would be appropriate to mention some geographical and climatic characteristics of the DAG site and Türkiye. While Türkiye is located between 26 - 45 degrees east longitude and 36 - 42 degrees north latitudes, the DAG site is located at an altitude of 3170 m on the Karakaya - Erzurum hill, at 39.78 degree north latitude and 41.23 degree east longitude. Besides, Türkiye has an average altitude of 1130 meters above sea level and annual average temperature values range between 3.6°C and 20.1°C [23]. The average annual precipitation and duration of sunshine for

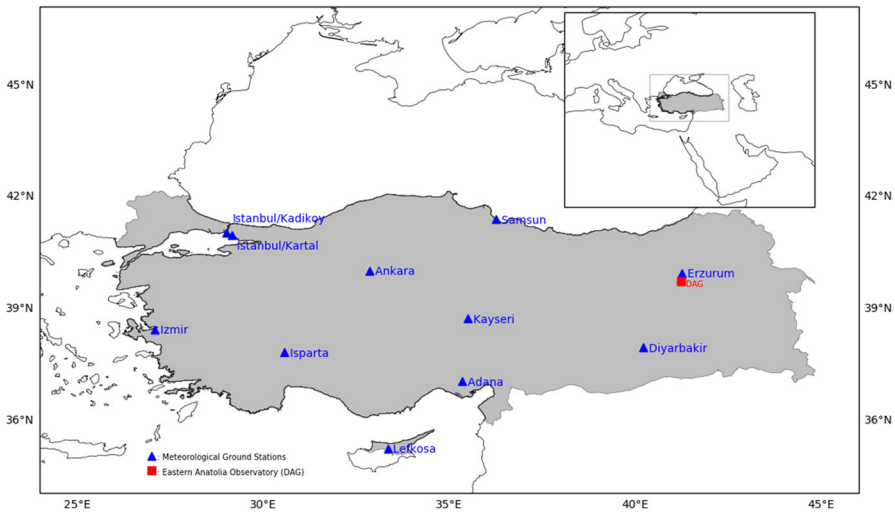


**Fig. 2** The locations of stations in the Türkiye's radiosonde network and DAG site. As can be seen from the map, RS stations are located to cover the whole country

Türkiye is approximately 648 mm and 6.9 hours per day, respectively. The average global solar radiation in Türkiye is also about  $4.2 \text{ kWhm}^2$  [24, 25]. The Mediterranean and Aegean coasts of Türkiye and the Marmara region have a Mediterranean climate, a continental climate in the interior, and a black sea climate in the black sea region [26, 27]. Continental climate characteristics are observed in Erzurum especially and winters are long and snowy, whereas summers are short and warm.

Türkiye has a radiosonde (RS) observation network with consisting of 11 meteorological stations. The meteorological station located in the city center of Erzurum has been conducting observations since 1929. Figure 2 shows the study areas along with the RS stations located in these regions. Based on observations spanning approximately 90 years<sup>1</sup>, the lowest temperature observed was  $-37.2^\circ\text{C}$  on December 28, 2002, while the highest temperature recorded was  $36.5^\circ\text{C}$  on August 11, 2006. According to TSMS records, the annual precipitation is approximately 432.2 mm. The least precipitation falls in the form of snow in winter, with approximately 50 days of snowfall. The snow cover period lasts approximately 114 days. The province receives the most precipitation in spring and summer [28]. The distance between the Türkiye RS stations was about 500 km on average. These RS stations were operated twice a day, 00:00 UTC and 12:00 UTC, as applied throughout the world. One of these stations (ERZM-17095) was located in the DAG near-region (Erzurum city center). The distance between the ERZM RS station and the DAG site was approximately 14 km.

In Table 1, the international station code (ID), city names, latitude, longitude, and elevation information of the ground stations of the TSMS used for validation are provided. These stations contain the distribution of all possible precipitable water vapor values based on various location characteristics (latitude, longitude, altitude) and different climatic zones.

<sup>1</sup> <https://www.mgm.gov.tr/veridegerlenen/il-ve-ilceler-istatistik.aspx?m=ERZURUM>

**Table 1** Information of radiosonde stations in Türkiye and Cyprus

ID	City	Latitude (N)	Longitude (E)	Elevation (m)
17351	Adana	37.00	35.34	27
17351	Ankara	39.97	32.86	891
17281	Diyarbakır	37.91	40.21	674
17095	Erzurum	39.91	41.25	1869
17240	Isparta	37.78	30.57	997
17064	İstanbul / Kadıköy	40.99	29.02	5
17064	İstanbul / Kartal	40.91	29.16	17
17220	İzmir	38.39	27.08	29
17196	Kayseri	38.69	35.50	1094
17030	Samsun	41.34	36.26	4
17516	Lefkoşa	35.20	33.35	100

Source: Türkiye State Meteorological Service

Using python and python’s siphon [29] and metpy [30] modules, RS data were downloaded from the University of Wyoming website<sup>2</sup> and were calculated using the following (1).

$$PWV = -\frac{1}{\rho_l g} \int_{P_{bottom}}^{P_{top}} r dp \tag{1}$$

where  $\rho_l$  is the density of water,  $g$  is the gravitational constant,  $r$  is the mixing ratio of water vapor and  $P_{bottom}$ ,  $P_{top}$  and  $p$  are the pressure of air [31].

An additional source of PWV data comes from meteorological satellites that employ remote sensing techniques. The indispensable role of geostationary satellites in delivering high temporal resolution is recognized. Consequently, PWV measurements sourced from the Spinning Enhanced Visible and Infrared Imager (SEVIRI) on the Meteosat Second Generation (MSG) satellites have been incorporated into the DAG database. This data set is included in the Satellite Application Facility on Support to Nowcasting and Very Short-Range Forecasting (NWC SAF) atmospheric stability collection and has been transmitted through TSMS FTP from early 2019.

The NWC SAF v2013 SEVIRI Physical Retrieval (SPhR) product, now known as iSHAI in v2018, was utilized in the study. This product encompasses subdatasets for the total precipitable water (TPW), layer precipitable water (LPW) vapor content (BL: Precipitable Water in the Boundary Layer, ML: Precipitable water in the middle layer and HL: Precipitable Water in the Upper Layer), along with instability indices (KI: K-Index, LI: Lifted Index and SHW: Showalter Index). BL, ML, and HL represent precipitable water vapor levels at pressure levels of 1000-850 hPa, 850-500 hPa, and 500 hPa to the top of the atmosphere, respectively. An example of a TPW image showing the work area is provided in Fig. 3.

Although TPW data are well known and are frequently used in meteorology and atmospheric sciences, this study provides new information for other disciplines such as

<sup>2</sup> <http://weather.uwyo.edu/upperair/sounding.html>

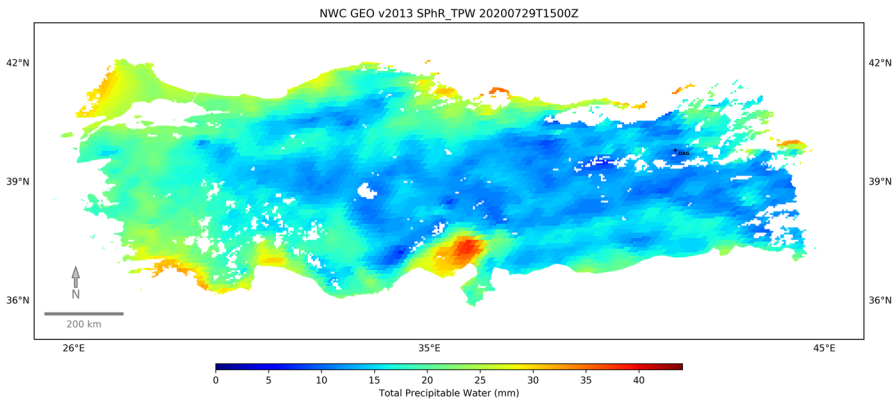


**Fig. 3** A representative exemplar of the NWC SAF TPW product (map) over Türkiye, captured on 2020-07-29 at 15:00 UTC

astronomy, hydrology, and agriculture. Another important point is that the reliability of the product has been demonstrated by a validation study of the TPW data at different points handled in Türkiye.

NWC SAF provides software used to produce a variety of atmospheric data for use in short-term weather forecasts. In Türkiye, TSMS produces atmospheric data for Türkiye and its surroundings using this software. SPhR data are generated by the TSMS and transmitted to DAG over the internet via FTP. The acquired data underwent a series of processing steps, including reprojection, georeferencing, and clipping, utilizing the capabilities of Python’s GDAL library. The Python libraries numpy, pandas, scipy, scikit-learn, cartopy, and matplotlib were used to perform tasks such as image processing, correlation analysis, and regression analysis, as well as to visualize the pixel values of satellite imagery.

The PWV values from the TSMS RS measurements and satellite imagery taken at 00:00 and 12:00 UTC were used to assess the accuracy of the NWC SAF TPW data. This product is produced by TSMS with a temporal resolution of 15 minutes and a spatial resolution of 3 km, covering Türkiye and its surrounding areas. PGE13 SPhR is based on the calculations of Jun for the GOES instruments [32, 33]. The development of PGE13 SPhR aims to achieve functional execution. The calculation focuses on observing the temperate climate and convective storms. The algorithm has only been applied to clear pixels or fields of interest (FOIs) with configurable width. The default number of FOI pixels was set to 3x3 [34].

### 3 Analysis method

In this study, correlation and regression analysis were used to evaluate the relationship between satellite imagery and radiosonde balloon retrievals. Regression analysis provides the mathematical expression of the relationship between two or more variables, while correlation analysis determines the direction (positive/negative) and strength of the relationship. Python programming language, “scipy.stats” module and “linregress”

function were used for analysis in the study. The “linregress” function calculates a linear least squares regression for two sets of measurements and returns the slope of the regression line, the intercept of the regression line, Pearson correlation coefficient, the p-value and the standard errors (for the slope and intercept). The slope of a line indicates its steepness, while the intercept indicates the point at which it intersects an axis. The slope and intercept define the linear relationship between the two variables and can be used to estimate the average rate of change. The p-value is a hypothesis test whose null hypothesis is that the slope is zero. It employs the Wald test with a t distribution of the test statistic. The reader can refer to the link below for more details<sup>3</sup>. Since PWV is a quantitative variable, it would be appropriate to use  $R^2$  (it is the coefficient of determination and the square of the Pearson correlation coefficient), MBE (mean bias error), MAE (mean absolute error), and RMSE (root mean square error) indexes to interpret the correlation and regression analysis.

Statistical parameters were used to determine the accuracy of the NWC SAF TPW product in the whole of Türkiye and to evaluate the results. Of these parameters,  $R^2$ , MBE, MAE, and RMSE are calculated using the expressions given in (2) to (6). In these expressions,  $n$  is the total number of data, and  $R_i$  and  $\bar{R}$  are the radiosonde PWV data and the average of these data, respectively.  $S_i$  and  $\bar{S}$  are the TPW data obtained from the satellite, and the average of these data.  $R^2$  represents the amount of variance explained by the independent variables in the model. The MBE is the average of the differences between the radiosonde PWV and the TPW values calculated from the satellite data. MBE provides information that the estimate made is higher or lower than the actual values. The MAE gives the average size of errors in a set of estimates without considering their direction. The RMSE is a quadratic error calculation rule that also measures the mean magnitude of the error. For high accuracy between the two quantities, the  $R^2$  value should be high (closer to one) and the MBE, MAE, and RMSE values should be low (closer to zero). For high accuracy between the two quantities, the  $R^2$  value should be high (closer to one) and the MBE, MAE, and RMSE values should be low (closer to zero). The minimum value of  $R^2$  is 0 and the maximum value is 1. In essence, the higher the accuracy of a model in making predictions, the closer its  $R^2$  will be to 1. Thus, when  $R^2$  is high and the MBE, MAE, and RMSE indices are low, it is decided that there is high agreement between the two quantities (satellite imagery and balloon data).

$$RS_{PWV} = m \times SP_{hR_{TPW}} + b \tag{2}$$

$$R^2 = \frac{[\sum_{i=1}^n (R_i - \bar{R})(S_i - \bar{S})]^2}{\sum_{i=1}^n (R_i - \bar{R})^2 \sum_{i=1}^n (S_i - \bar{S})^2} \tag{3}$$

$$MBE = \frac{1}{n} \sum_{i=1}^n (R_i - S_i) \tag{4}$$

<sup>3</sup> <https://docs.scipy.org/doc/scipy/reference/generated/scipy.stats.linregress.html>

$$MAE = \frac{1}{n} \sum_{i=1}^n |R_i - S_i| \quad (5)$$

$$RMSE = \sqrt{\frac{1}{n} \sum_{i=1}^n (R_i - S_i)^2} \quad (6)$$

In this study, the pixel values of the NWC SAF images at the TSMS ground station locations were used for validation, while the pixel values at the DAG site were used for time series analysis. The NWC SAF TPW data has a temporal resolution of 15 minutes due to RS measurements being taken twice daily (at 00:00 and 12:00 UTC). To ensure consistency in measurement times, only the 00:00 and 12:00 UTC measurements of the NWC SAF TPW data were used for validation. This allowed for a spatial and temporal comparison of the two datasets.

## 4 Results and discussion

Prior to performing the correlation analysis, the statistical information of the dataset compiled from radiosonde and satellite data for the reference stations is presented in Table 2. Upon examining of the Table 2, it is evident that both the night and day time SPhR and RS data exhibit similar values. The analysis of the minimum values reveals that a slightly higher value of 2.19 mm is calculated in the RS day time measurement while the two data sources display similar values. The comparison of the maximum values shows that the SPhR values are 7 mm and 5 mm higher than the RS values for day time and night time, respectively. There is an approximate difference of 1.5 mm between the mean and median values, with the mean values higher than the median values. Although the SPhR mean values at night are lower than the RS mean values, the opposite is observed for day time. The examination of the standard deviation in the table indicates a high calculation for the SPhR daytime, suggesting that the SPhR TPW values are measured in a wider range and larger values during the daytime. This observation is consistent with results from other indices presented in the table.

The results of the correlation analysis are presented in Table 3, where  $m$  and  $b$  are slope and intercept of the regression line represent the coefficients between the SPhR and RS PWV values. As far as the examination of the  $R^2$  values in the table

**Table 2** Statistics of all reference station data

Quantities	SPhR (mm)	RS (mm)	SPhR (mm)	RS (mm)
Count	1925	1925	1637	1637
Minimum	1.76	1.86	1.76	2.19
Maximum	49.41	44.52	51.18	44.07
Mean	16.59	17.60	17.11	16.71
Media	15.29	16.23	15.29	15.03
Std. Dev.	8.65	8.84	9.09	8.66



**Table 3** Statistics of the correlation analysis between SPhR TPW and RS PWV

ID	City	Time	m	b	$R^2$	MBE (mm)	MAE (mm)	RMSE (mm)
17030	Samsun	00 UTC	1.09	0.09	0.95	2.01	2.35	2.90
17030	Samsun	12 UTC	1.02	0.38	0.94	0.83	1.68	2.17
17064	İstanbul	00 UTC	0.99	0.81	0.93	0.56	1.51	2.01
17064	İstanbul	12 UTC	0.94	0.54	0.91	-0.78	1.64	2.21
17095	Erzurum	00 UTC	1.14	-0.23	0.91	1.07	1.36	1.87
17095	Erzurum	12 UTC	1.01	0.73	0.83	0.85	1.32	1.88
17196	Kayseri	00 UTC	0.99	0.63	0.90	0.53	1.20	1.75
17196	Kayseri	12 UTC	0.99	-0.28	0.84	-0.37	1.20	2.08
17240	Isparta	00 UTC	1.09	0.78	0.94	1.98	2.06	2.44
17240	Isparta	12 UTC	0.94	1.10	0.88	0.41	1.17	1.57
17351	Adana	00 UTC	0.99	0.34	0.92	-0.02	1.82	2.71
17351	Adana	12 UTC	0.93	-0.28	0.91	-2.07	2.61	3.44

was concerned, the lowest coherence is observed at 17095-Erzurum 12:00 UTC (0.83) and 17196-Kayseri 12:00 UTC (0.84) while the highest coherence is found at 17030-Samsun (day and night; 0.95 and 0.94) and 17240-Isparta 00:00 UTC (0.95). The cities of Erzurum and Kayseri stations, which exhibit the lowest correlation, share common characteristics such as being far from sea influence, having high altitudes, and low PWV values. Considering that the MSG satellites (MSG-4 or Meteosat-11) carries the SEVIRI sensor, which produces the SPhR product, and is located at 0 degrees longitude, the farthest radiosonde station from the satellite sub-point is Erzurum. This distance may affect the correlation at the Erzurum station. Stations with high consistency, except Isparta, share common features such as proximity to the sea and high PWV values.  $R^2$  values ranging from 0.83 to 0.95 were calculated for the reference stations. These values indicate a strong statistical relationship, demonstrating the reliability and accuracy of the SPhR TPW data on Türkiye.

When examining the MBE values in Table 3, it is observed that they range from -2.07 mm to 2.01 mm. The negative MBE values indicate that the TPW data generally measured higher than the RS data while the positive MBE values indicate that the TPW data generally measured lower than the RS data. The TPW values were predominantly higher than RS PWV values at the 17351-Adana station, as well as at the 17064-İstanbul (day time) and 17196-Kayseri (day time) stations. The MAE and RMSE values in the Table 3 range from 1.17-2.61 mm and 1.57-3.44 mm, respectively. Similar values were observed at other stations. The lowest (best) MAE and RMSE values were recorded at 17240-Isparta at 12:00 UTC, while the highest (worst) correlation was observed at 12:00 UTC at the 17351-Adana station. Higher MAE values were calculated during the day time compared to night time at the İstanbul and Adana stations while higher MAE values were calculated at night time compared to day time at the Samsun, Isparta, and Erzurum stations. In terms of RMSE values, the night time values were higher than the day time values at the Samsun and Isparta stations while day time values were higher than night time values at the other stations. In

terms of astronomical observations, especially for night time, reliable accuracy and high temporal resolution PWV data will determine the accuracy and precision of IR observations.

In Fig. 4 (night time) and Fig. 5 (day time), the distribution of SPhR TPW and RS PWV data from the reference stations is presented. All graphs clearly show a consistent distribution of both PWV values. High PWV values were observed at Samsun, Istanbul, and Adana while the relatively low PWV values were recorded at the Erzurum, Kayseri, and Isparta stations. The common characteristic of stations with low PWV values is their high altitude. The Erzurum meteorology station, located at an altitude of 1869 meters, records lower PWV values compared to other regions. The establishment of the DAG in Konaklı/Erzurum at an altitude of 3170 meters offers a notable benefit by reducing PWV values and minimizing negative atmospheric impacts on astronomical observations.

Figure 6 displays the aggregated distribution patterns of all stations throughout the day time and night time, revealing a comparable trend with marginally greater consistency ( $R^2 = 0.94$ ) observed at night time.

Given these considerations, the SPhR TPW data, which were validated earlier, demonstrate a strong correlation with the radiosonde measurements. The utilization of TPW data for IR astronomy at the DAG site is expected to be highly beneficial due to their precision, temporal resolution, and accuracy. Consequently, the PWV measurements at the DAG site have been analyzed over time using SPhR TPW data.

In Fig. 7, the time series of SPhR TPW values for the DAG site are presented at 15 minutes intervals, hourly, daily, and monthly. The upper left panel of Fig. 7 displays the instantaneous SPhR TPW values obtained from the 15 minutes images of the DAG site. The hourly median TPW values derived from these 15 minutes values are shown in the upper right panel while the daily median TPW values are presented in the lower left panel, and the monthly median TPW values are shown in the lower right panel of Fig. 7. The 15 minutes TPW pattern for the DAG site is illustrated in Fig. 7. It is evident from the figure that data transmission was interrupted in early 2020, resulting in missing data. This lack of data will have a slight impact on the statistical analysis of the dataset.

As shown in Fig. 7, the mean values of total precipitable water vapor are higher in the summer season compared to the winter season. The dataset for this study only included one winter season, which may explain the relatively high TPW statistics. Future studies with a wider date range are expected to yield lower statistical values. The hourly median TPW data distribution is similar to the previous plot, with higher values observed in summer and lower values in winter. Daily TPW values were calculated taking the median of 15 minutes TPW values, with minimum and maximum values ranging from 2–14 mm. The monthly median TPW values were also calculated from the 15-minute TPW values, showing values varying from about 3–10 mm. The monthly TPW values for DAG generally show a decreasing trend from June to January, followed by an increase in the first seven months of 2020. TPW values decreased from July to the end of the year. In particular, on winter days with low TPW, favorable conditions in other atmospheric parameters such as cloud cover, temperature, and wind speed will enable high-quality astronomical observations.

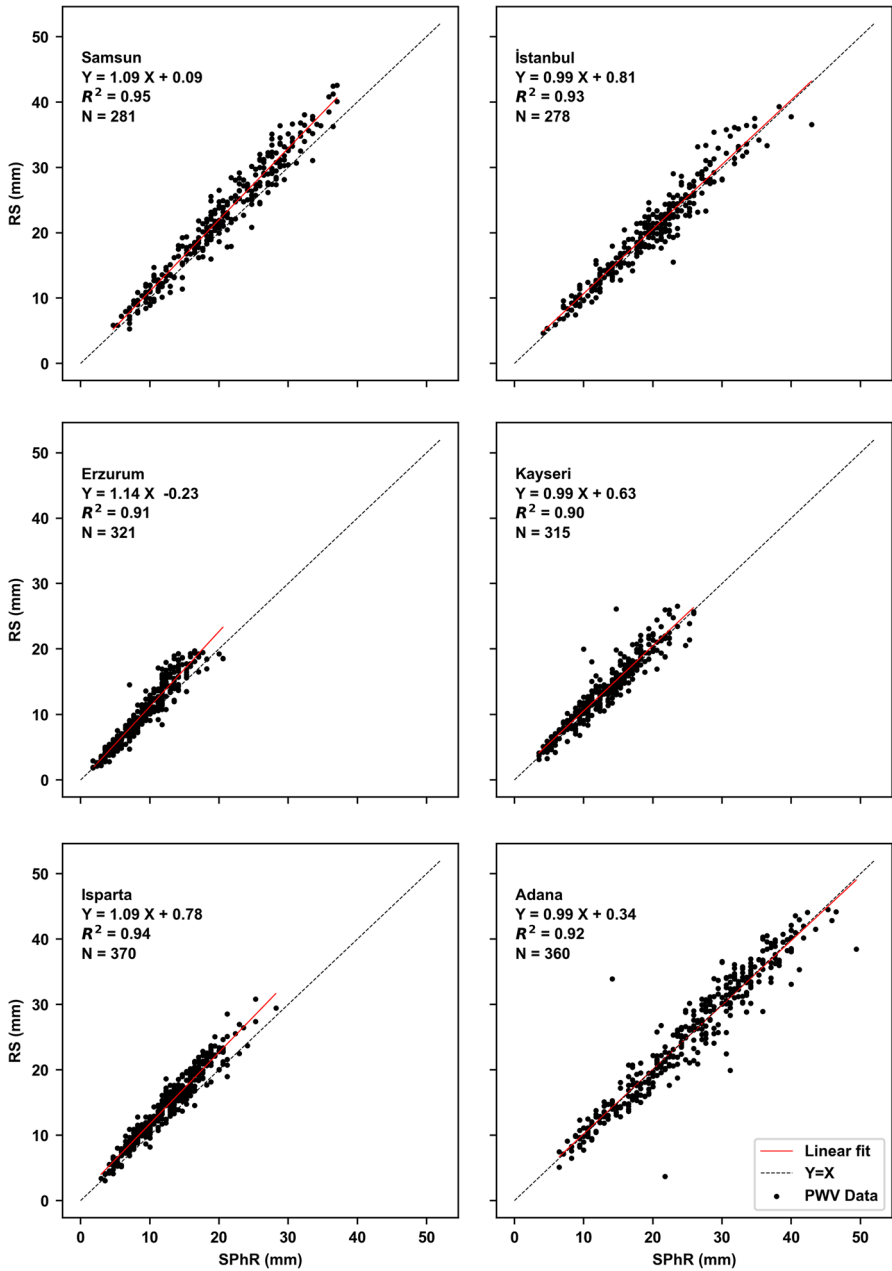


Fig. 4 Scatter plots of six reference stations (00:00 UTC). RS and SPhR comparison was made for these stations. The  $R^2$  values range between the lowest 0.9 and the highest 0.95

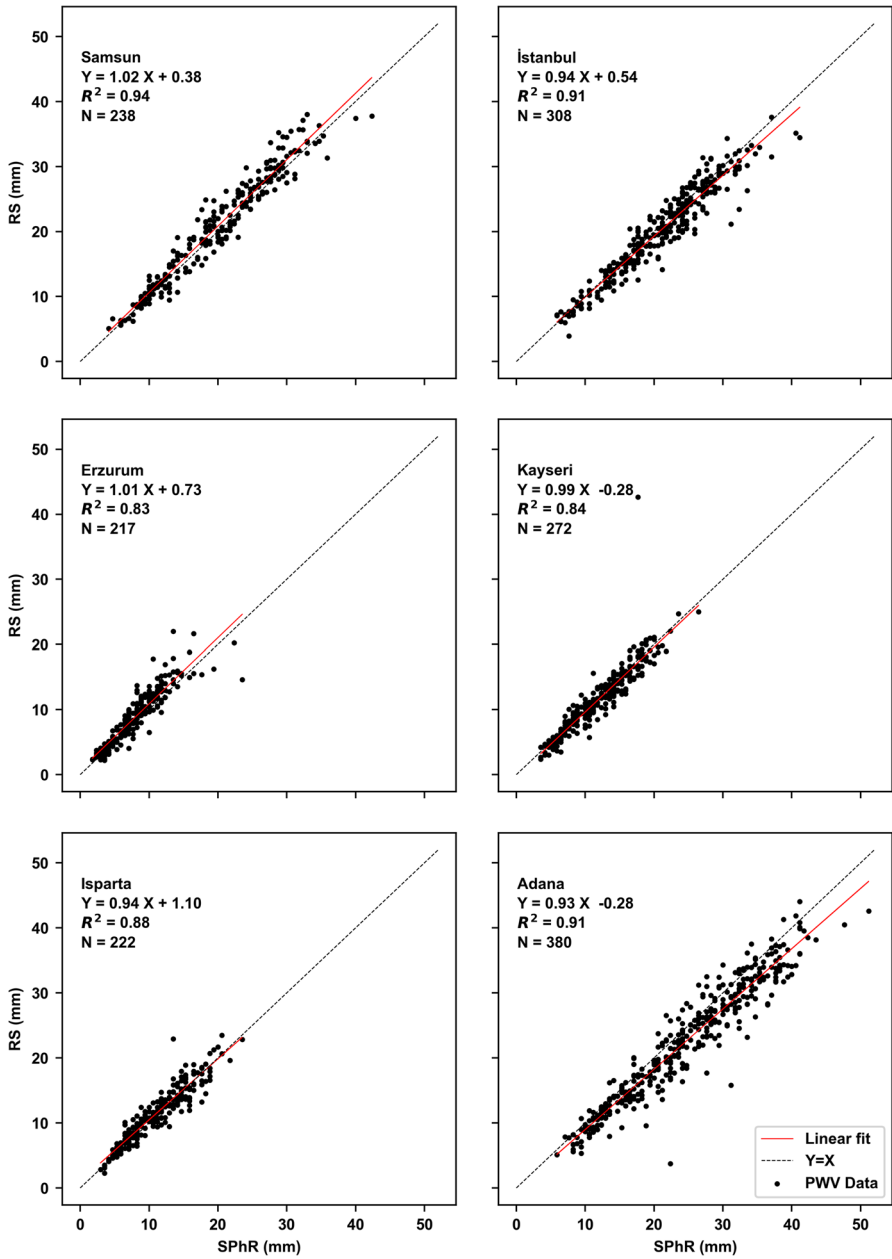
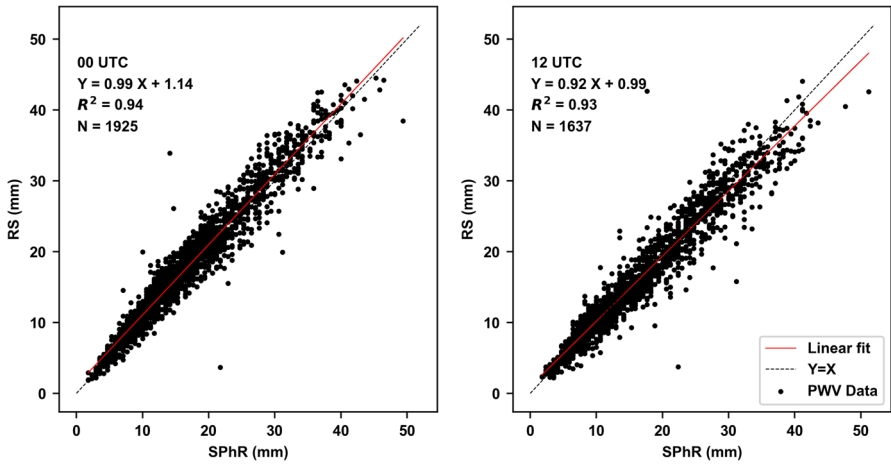
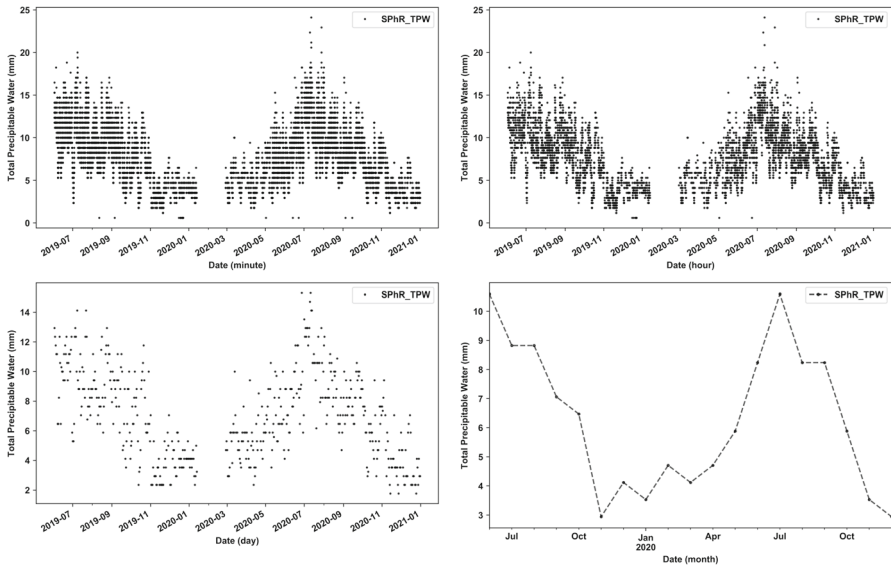


Fig. 5 Scatter plots of six reference stations (12:00 UTC). RS and SPhR comparison was made for these stations. The  $R^2$  values range between the lowest 0.83 and the highest 0.94



**Fig. 6** Scatter plots of all reference stations at the nighttime (00:00 UTC) and daytime (12:00 UTC). The  $R^2$  values are 0.94 for nighttime and 0.93 for daytime

The PWV indices relevant to infrared astronomical observations are systematically classified into four distinct categories [2]: (1)  $PWV < 3$  mm, considered good or excellent; (2)  $3 \leq PWV < 6$  mm, classified as fair or mediocre; (3)  $6 \leq PWV < 10$  mm, classified as poor; and (4)  $PWV \geq 10$  mm, considered extremely poor. Low PWV values are conducive to detailed observations, such as direct imaging of exoplanets and optimal planning of observation times during nights with favorable conditions.



**Fig. 7** 15-minute (Upper Left), Hourly (Upper Right), Daily (Lower Left) and Monthly (Lower Right) SPhR TPW data over DAG site

The use of precise atmospheric data during the planning phase of astronomical observations is crucial for making accurate decisions. The PWV values in the tables are derived from the values of the closest pixel to the location of the DAG site in all 15 minutes NWC SAF images. During the study period, the mean and median PWV values at the DAG site were approximately 7 mm with the minimum and maximum values calculated as 0.59 mm and 24.12 mm, respectively.

In a separate study, the GNSS meteorology method was used to evaluate precipitable water vapor at the DAG site [35]. Statistical results from the collected data (October 2016 to June 2017) reported an average PWV of 3.2 mm and a median of 2.7 mm. A comparison with these results shows a slight increase in the PWV measurement values in this study. The slight difference in PWV measurements between the studies can be attributed to the different data collection periods; the previous study covered one winter and one summer season using the GNSS meteorology method, whereas this study included one winter and two seasons. Figure 7 shows that PWV measurements are generally higher during the summer months than in the winter months. It is imperative to emphasize that the selection of data collection intervals significantly impacts the research findings and, according to the criteria established by [36], the PWV values at the DAG site are considered suitable for infrared observations.

The statistics of the TPW datasets are as follows: The dataset has a total count of **27,260** images. The recorded minimum value is **0.59 mm**, while the maximum value is **24.12 mm**. The mean value is **7.10 mm** and the median is **7.06 mm**. In addition, the standard deviation is **3.14 mm**.

This section of the research demonstrates the quantification of near-surface water vapor depletion at the DAG site. In this study, atmospheric data from three distinct layers were gathered using the SPhR product. During the early stages of the study, the reliability of the product was evaluated and shown to be very accurate.

The DAG site is characterized by an average pressure level of 700 hPa. Based on the atmospheric conditions of the DAG site, a significant amount of water vapor that has accumulated within a vertical column in the atmosphere would be expected to undergo removal. Figures 7 and Table 4 provide information on the current situation. The distribution of all precipitable water vapor values was obtained from 15 minutes satellite images.

During the study period, a value of 0.29 mm was observed in BL images in 16 instances out of a total of 50932 satellite images. This recurring value may be attributed to the measurement error and can be excluded from the analysis. From this perspective,

**Table 4** Statistics of layer precipitable water over the DAG site

Quantities	BL (mm)	ML (mm)	HL (mm)	TPW (mm)	TPW (mm) [3x3 mean]
Count	16	25391	25391	25391	25391
Minimum	0.29	0.38	0.07	0.59	0.59
Maximum	0.29	21.93	2.49	24.12	24.47
Mean	0.29	6.57	0.48	7.05	7.61
Median	0.29	6.43	0.40	7.06	7.45
Std. Dev.	0.00	2.97	0.30	3.13	3.35

it can be conclusively asserted that the DAG site has been shielded from the influence of the planetary boundary layer with respect to water vapor. The analysis of the red color distribution in the graph and the “HL” column data from the table indicates that the air mass above 500 hPa over the DAG telescope has an average precipitable water vapor of 0.48 mm.

The observation plans for astronomical observations should be made when low values of precipitable water vapor are measured at a site, as the PWV values above 10 mm are not optimal for astronomical observations. During the dry season, it is observed that both lower and upper level water vapor values are relatively low when the vertical distribution of water vapor is analyzed at the DAG site. The primary contribution to precipitable water vapor that could impact astronomical observations is found in the middle layer of the atmosphere, particularly between 700-500 hPa.

The DAG is established on the Karakaya Hills in an area with many hills and mountain range. Because the DAG telescope will observe at a zenith angle of 0-70 degrees, the air masses around the site remain in the field of view of the telescope. In terms of terrain structure, meteorological conditions can vary significantly within a few kilometers. In order to understand the severity of changes in these meteorological parameters, the site must be evaluated together with its environment.

The previous investigations at the DAG site included a vertical analysis of water vapor. In order to examine the PWV for all directions, we need that the water vapor concentrations how vary spatially within the DAG site. The results of these types of analysis are presented in Fig. 8 and Table 5. The graphs display the Total Precipitable Water (TPW) values of a single pixel (1x1) at the location of the DAG telescope as well as the values of the nine surrounding pixels (TPW [3x3 mean]) and their differences.

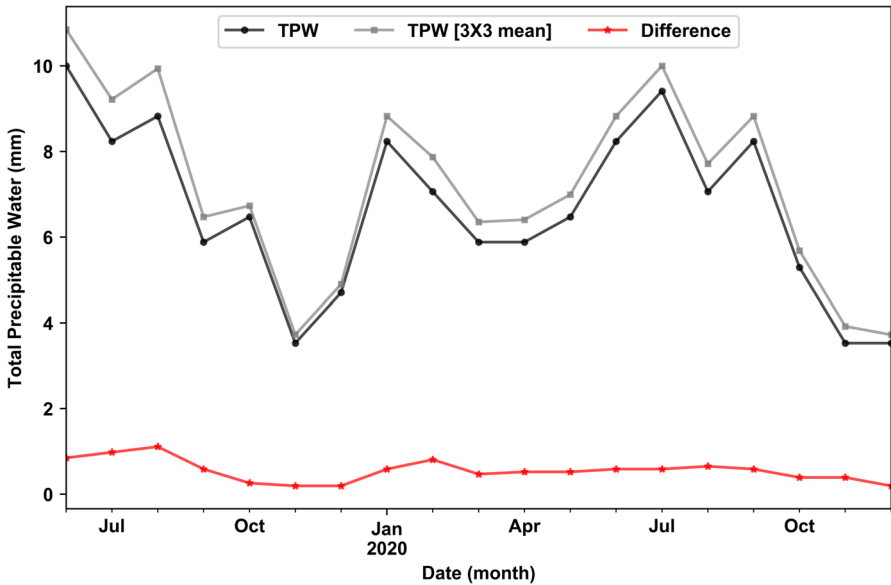


Fig. 8 TPW values of different pixels over the DAG site. Distribution of precipitable water layer data on the DAG site across the entire dataset (June 2019 - Dec 2020)

**Table 5** Statistics of layer precipitable water vapor over Türkiye

Layer	Minimum	Maximum	Mean	Median	Std. Dev.
BL	0.0022	16.651	3.5829	2.6588	3.5276
ML	0.3781	15.5817	9.3762	9.5287	0.9735
HL	0.0672	0.69	0.4571	0.4556	0.0359
TPW	0.5882	29.8505	13.3491	12.9143	3.3717

In the eastern regions of Türkiye, the SEVIRI sensor reaches approximately 5 km pixel resolution. Therefore, the area is covered by a single pixel of size approximately  $25 \text{ km}^2$ . Furthermore, the total area covered by nine pixels approximates  $225 \text{ km}^2$  (15 km by 15 km).

At this stage of the study, the PWV values of the DAG site and its surroundings were compared. The plot graphs of this comparison are shown in Fig. 8. In the figure, the black line plot shows the value of a single pixel, the gray line plot shows the value of 3x3 pixels, and the red line plot shows their differences.

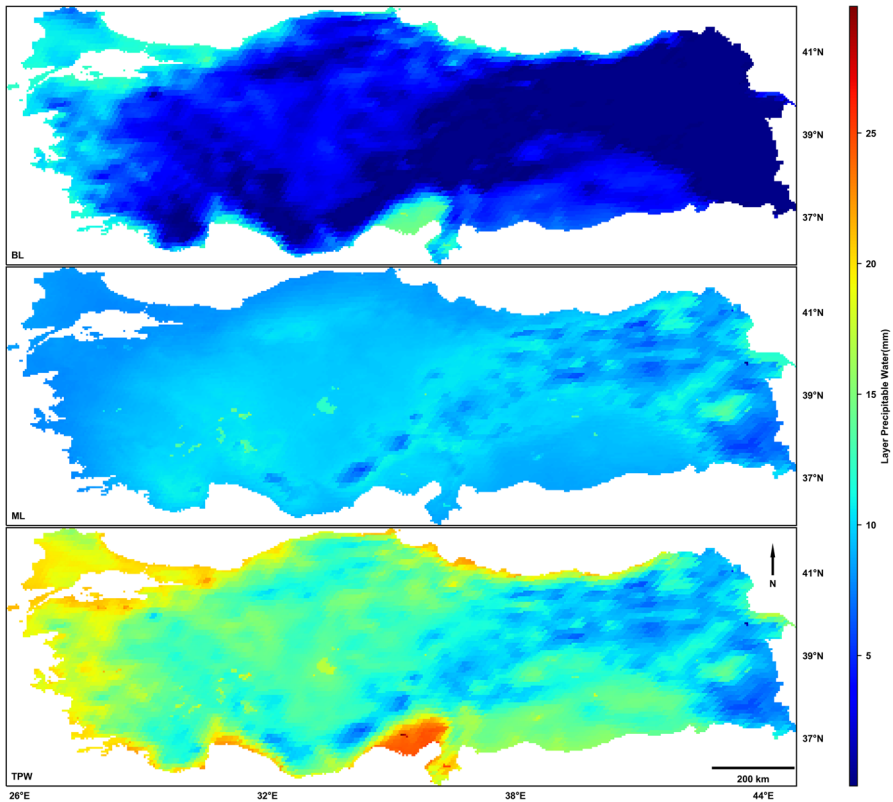
The mean precipitable water vapor measurements indicate values of **7.05 mm for the 1x1 pixel** and **7.61 mm for the 3x3 pixel region**. A comparable disparity was also observed in the median measurements. Although the minimum values recorded for both areas were identical at **0.59 mm**, a **0.35 mm** discrepancy was observed in the maximum values. In the datasets depicted in the graphical representations and tabular format, it becomes apparent that the precision of site selection surpasses that of the adjacent regions on the hill where the observatory is located.

Figure 9, the precipitable water vapor values for the three different layers (boundary layer, mid layer, and total) are displayed as maps. The maps represent Türkiye's nighttime PWV as only nighttime values were used in producing them, because astronomical observations were conducted at night.

Table 5 presents the statistics of the PWV values for both the sea level and the mountain regions. The HL values are not comparable to other layer values, so they are not displayed as a map. This inconsistency is similarly observable in the table. Upon jointly reviewing the table and maps, it becomes clear that there is a marked disparity in the distribution of water vapor between the sea level and the mountainous areas of Türkiye. In addition, attributed to the modulation of altitude in precipitable water vapor and the elevated terrain in eastern Türkiye, it is manifest that the PWV values exhibit a decreasing trend from the western to the eastern regions of the country.

Upon the examination of the boundary layer (BL) map depicted in Fig. 9, it becomes evident that elevated concentrations of water vapor predominantly characterize the coastal areas of Türkiye at sea level. In contrast, the central and southeastern territories of Türkiye display diminished Precipitable Water Vapor values, with the PWV metrics registering as nil in the Mediterranean and Eastern Anatolia regions, attributable to the elevated altitudes. Further examination of the Mixing Layer (ML) map reveals that regions situated at higher altitudes manifest lower PWV values relative to other areas. In contrast, PWV values at sea level, particularly along the coastal zones of Türkiye, are comparatively low.





**Fig. 9** Three different layers PWV maps over Türkiye

In the middle of Fig. 9, lakes and plains are identified as areas with high PWV values on the ML map. The TPW map, which shows the total PWV values in all layers, serves as the final PWV map of Türkiye during the study period. The map patterns for the other layers are also shown in this map. It is evident when all maps are taken into account that PWV values tend to accumulate at lower levels of the atmosphere.

In the DAG site, the lowest PWV value (equal to zero) is in the boundary layer (BL), with similar PWV values (ranging between 0.07 mm and 0.48 mm) in the upper layers. The eastern regions of Türkiye, particularly mountainous areas, typically have lower PWV values. This is because humid air releases moisture as it ascends, leading to decreased PWV values, which signify lower humidity and drier weather conditions. Analysis of the maps in Fig. 9 reveals that settlements situated at higher altitudes, such as DAG, have significantly lower PWV levels compared to those at sea level. Therefore, it is highly consistent with statistical data that the selection of observatory sites in these areas is preferred. As a result, it can be inferred that conducting highly sensitive activities such as astronomical infrared observations at higher altitudes would result in less atmospheric interference. It is evident that the mean PWV value observed at the DAG observatory is less than 10 mm in all layers.

## 5 Conclusion

In this research, we presented our initial findings on the PWV content at the DAG site to enhance our understanding of the site's atmospheric characteristics, especially DAG, which houses Türkiye's largest telescope with a diameter of 4 meters and is the first near-infrared (NIR) telescope in the country, is planning to achieve first light in late summer in 2024.

This research aimed to explore the impact of water vapor on infrared astronomical observations using DAG telescopes. The effective monitoring of PWV would result in the generation of higher-quality astronomical observation products in the IR region and a reduction in the operating cost of the devices used at the site. In this regard, PWV values have been analyzed in three parts. The initial assessment focused on evaluating the accuracy of the satellite imagery data used. This step is crucial to ensure that subsequent analyses, such as temporal and spatial evaluations, are based on accurate and reliable data. Subsequently, a temporal analysis was performed on the DAG site using satellite-derived data. Lastly, the study conducted a spatial analysis of PWV data values across Türkiye, considering stratification into atmospheric layers (low, medium, and high). The main findings of the study are listed below.

- The TPW dataset was initially validated at six radiosonde stations in Türkiye. The validation results showed that the SPhR TPW data with a 15 minutes temporal resolution had a strong relationship ( $R^2 > 80$ ) with radiosonde data at both day time and night time.
- The correlation analysis yielded  $R^2$  values between 0.83-0.95 for day and night time for the reference stations considered. This indicates a strong statistical relationship and the reliability of the SPhR TPW data across Türkiye.
- The mean bias error values between the SPhR TPW and radiosonde data vary ranged from -2.07 mm to 2.01 mm. This means that the SPhR TPW data measured on average about 2 mm of small or large. This measurement error is a relatively acceptable amount. Also The SPhR TPW data generally showed lower values compared to the radiosonde measurements.
- Temporal analysis of SPhR TPW data was performed for the DAG site from June 2019 to 2020. During the study period, the mean and median TPW values at the DAG site were approximately 7 mm and minimum and maximum values were calculated as 0.59 mm and 24.12 mm.
- Additionally, higher TPW values were observed in the DAG area during the summer months, while lower TPW values were observed in the winter months.
- Monthly median TPW values at the DAG site varied between approximately 3-10 mm, with a decreasing trend from June to January and an increase in the first seven months of 2020.
- Spatial and vertical analysis of precipitable water vapor data was conducted over DAG site and Türkiye from SPhR data. The results show that the values of the DAG site remain low compared with those of its surroundings.
- The lower and upper-level water vapor values are quite low and the main contribution comes from the middle layer of the atmosphere especially 700-500 hPa.

**Acknowledgements** This research is supported by Türkiye National Observatories, ATASAM-DAG (Astrophysics Research and Application Center and the Eastern Anatolia Observatory, Project No: 2011K120230) by means of infrastructure and personnel. In addition, we would like to thank the Turkish State Meteorological Service (TSMS) and the NWC SAF for providing data for this study.

**Author Contributions** Conceptualization: Kazım Kaba, Recep Balbay, Cahit Yeşilyaprak Methodology: Recep Balbay, Kazım Kaba, Süleyman Fişek Formal analysis and investigation: Recep Balbay, Kazım Kaba, Süleyman Fişek Writing - original draft preparation: Recep Balbay, Kazım Kaba Writing - review and editing: Recep Balbay, Kazım Kaba, Süleyman Fişek, Cahit Yeşilyaprak Supervision: Kazım Kaba, Cahit Yeşilyaprak

**Funding** Open access funding provided by the Scientific and Technological Research Council of Türkiye (TÜBİTAK). The authors declare that they have received no funding support.

**Data Availability** Radiosonde data were taken from the University of Wyoming, College of Engineering, Department of Atmospheric Science “Atmospheric Soundings” (<https://weather.uwyo.edu/upperair/sounding.html>) Web page for the relevant region and dates. NWC SAF satellite data was received through a special protocol signed between ATASAM-DAG and TSMS.

**Code Availability** Code is available upon request.

## Declarations

**Conflict of interest/Competing interests** The authors declare that they have no conflict of interest.

**Consent for publication** The authors confirm that this article has not been previously published in any journal.

**Materials availability** Materials are available upon request.

**Open Access** This article is licensed under a Creative Commons Attribution 4.0 International License, which permits use, sharing, adaptation, distribution and reproduction in any medium or format, as long as you give appropriate credit to the original author(s) and the source, provide a link to the Creative Commons licence, and indicate if changes were made. The images or other third party material in this article are included in the article’s Creative Commons licence, unless indicated otherwise in a credit line to the material. If material is not included in the article’s Creative Commons licence and your intended use is not permitted by statutory regulation or exceeds the permitted use, you will need to obtain permission directly from the copyright holder. To view a copy of this licence, visit <http://creativecommons.org/licenses/by/4.0/>.

## References

1. Brunetti, M., Prodi, F.: The climate system. EPJ Web Conf. **98**, 02001 (2015). <https://doi.org/10.1051/epjconf/20159802001>
2. García-Lorenzo, B., Eff-Darwich, A., Castro-Almazán, J., Pinilla-Alonso, N., Muñoz-Tuñón, C., Rodríguez-Espinosa, J.M.: Infrared astronomical characteristics of the Roque de los Muchachos Observatory: precipitable water vapour statistics. Mon. Not. R. Astron. Soc. **405**(4), 2683–2696 (2010). <https://doi.org/10.1111/j.1365-2966.2010.16649.x>
3. Villanueva, G.L., Smith, M.D., Protopapa, S., Faggi, S., Mandell, A.M.: Planetary spectrum generator: an accurate online radiative transfer suite for atmospheres, comets, small bodies and exoplanets. J. Quant. Spectrosc. Radiat. Transfer **217**, 86–104 (2018). <https://doi.org/10.1016/j.jqsrt.2018.05.023>
4. Sarazin, M., Kerber, F., Breuck, C.: Precipitable water vapour at the eso observatories: the skill of the forecasts. The Messenger 17–21 (2013)

5. Pérez-Jordán, G., Castro-Almazán, J.A., Muñoz-Tuñón, C., Codina, B., Vernin, J.: Forecasting the precipitable water vapour content: validation for astronomical observatories using radiosoundings. *Mon. Not. R. Astron. Soc.* **452**(2), 1992–2003 (2015). <https://doi.org/10.1093/mnras/stv1394>
6. Wirth, L.H.A.: Product tutorial on total precipitable water content products. [https://resources.eumetrain.org/data/3/359/print\\_2.htm](https://resources.eumetrain.org/data/3/359/print_2.htm)
7. Colavita, M.M., Swain, M.R., Akeson, R., Koresko, C., Hill, R.: Effects of atmospheric water vapor on infrared interferometry. *Publ. Astron. Soc. Pac.* **116**(823), 876–885 (2004). <https://doi.org/10.1086/424472>
8. Peixoto, J., Oort, A.H.: The climatology of relative humidity in the atmosphere. *J. Clim.* **9**(12), 3443–3463 (1996). [https://doi.org/10.1175/1520-0442\(1996\)009<3443:TCORHI>2.0.CO;2](https://doi.org/10.1175/1520-0442(1996)009<3443:TCORHI>2.0.CO;2)
9. Held, I., Soden, B.: Water vapor feedback and global warming. *Annual Review of Energy and The Environment - ANNU REV ENERG ENVIRON* **25**, 441–475 (2000). <https://doi.org/10.1146/annurev.energy.25.1.441>
10. Turchi, A., Masciadri, E., Pathak, P., Kasper, M.: High-accuracy short-term precipitable water-vapour operational forecast at the very large telescope and perspectives for sky background forecast. *Mon. Not. R. Astron. Soc.* **497**(4), 4910–4920 (2020). <https://doi.org/10.1093/mnras/staa2210>
11. Tremblin, P., Schneider, N., Minier, V., Durand, G., Urban, J.: Worldwide site comparison for submillimetre astronomy. *Astron. Astrophys.* **548**, 65 (2012). <https://doi.org/10.1051/0004-6361/201220420>
12. Giovanelli, R., Darling, J., Henderson, C., Hoffman, W.F., Barry, D.C., Cordes, J., Eikenberry, S.S., Gull, G.E., Keller, L.D., Smith, J.D., Stacey, G.J.: The optical/infrared astronomical quality of high altitude sites. II. infrared characteristics. *Publications of the Astronomical Society of the Pacific* **113**(785), 803–813 (2001). <https://doi.org/10.1086/322136>
13. Marin, J., Pozo, D., Cure, M.: Estimating and forecasting the precipitable water vapor from GOES satellite data at high altitude sites. *Astron. Astrophys.* **573**, 41 (2014). <https://doi.org/10.1051/0004-6361/201424460>
14. Wood-Vasey, W.M., Perrefort, D., Baker, A.: GPS measurements of precipitable water vapor can improve survey calibration: a demonstration from KPNO and the mayall z-band legacy survey. *Astron. J.* **163**(6), 283 (2022). <https://doi.org/10.3847/1538-3881/ac63bb>
15. Lorenzo, B., eff-darwich, A., Castro-Almazán, J., Pinilla-Alonso, N., Munoz-Tunon, C., Rodriguez Espinosa, J.: Infrared astronomical characteristics of the roque de los muchachos observatory: precipitable water vapour statistics. *mnras* **405**, 2683–2696 (2010). <https://doi.org/10.1111/j.1365-2966.2010.16649.x>
16. Otarola, A., Travouillon, T., Schöck, M., Els, S., Riddle, R., Skidmore, W., Dahl, R., Naylor, D., Querrel, R.: Thirty meter telescope site testing x: precipitable water vapor. *Publ. Astron. Soc. Pac.* **122**(890), 470–484 (2010). <https://doi.org/10.1086/651582>
17. Yesilyaprak, C., Keskin, O., Jolissaint, L.: Eastern anatolia observatory (dag): the status in 2022, towards the first light. In: *Ground-based and Airborne Telescopes IX*, vol. **12182**, pp. 121–125. SPIE, ??? (2022). <https://doi.org/10.1117/12.2630889>
18. King, M.D., Menzel, W.P., Kaufman, Y.J., Tanre, D., Gao, B.-C., Platnick, S., Ackerman, S.A., Remer, L.A., Pincus, R., Hubanks, P.A.: Cloud and aerosol properties, precipitable water, and profiles of temperature and water vapor from modis. *IEEE Trans. Geosci. Remote Sens.* **41**(2), 442–458 (2003). <https://doi.org/10.1109/TGRS.2002.808226>
19. Zhao, Q., Zhang, X., Wu, K., Liu, Y., Li, Z., Shi, Y.: Comprehensive precipitable water vapor retrieval and application platform based on various water vapor detection techniques. *Remote Sensing* **14**(10) (2022). <https://doi.org/10.3390/rs14102507>
20. He, J., Liu, Z.: Comparison of satellite-derived precipitable water vapor through near-infrared remote sensing channels. *IEEE Trans. Geosci. Remote Sens.* **57**(12), 10252–10262 (2019). <https://doi.org/10.1109/TGRS.2019.2932847>
21. Zhao, Q., Ma, X., Yao, W., Liu, Y., Yao, Y.: A drought monitoring method based on precipitable water vapor and precipitation. *J. Clim.* **33**(24), 10727–10741 (2020). <https://doi.org/10.1175/jcli-d-19-0971.1>
22. Seidel, D.J., Sun, B., Pettey, M., Reale, A.: Global radiosonde balloon drift statistics. *Journal of Geophysical Research* **116**(D7) (2011). <https://doi.org/10.1029/2010jd014891>
23. Deniz, A., Toros, H., Incecik, S.: Spatial variations of climate indices in turkey. *Int. J. Climatol.* **31**(3), 394–403 (2011). <https://doi.org/10.1002/joc.2081>

24. Iyigun, C., Türkeş, M., Batmaz, İ., Yozgatligil, C., Puruçcuoğlu, V., Koç, E.K., Öztürk, M.Z.: Clustering current climate regions of turkey by using a multivariate statistical method. *Theoretical and Applied Climatology* **114**(1), 95–106 (2013). <https://doi.org/10.1007/s00704-012-0823-7>
25. Kaba, K., Yeşilyaprak, C.: Cm saf oransal bulut kapallılığı (cfc) verisinin başarımı ve doğu anadolu gözlemevi (dag) yerleşkesi için analizi. *Journal of Advanced Research in Natural and Applied Sciences* **7**, 304–318 (2021). <https://doi.org/10.28979/jarnas.871585>
26. Kaba, K., Sarıgül, M., Avcı, M., Kandırımaz, H.M.: Estimation of daily global solar radiation using deep learning model. *Energy* **162**, 126–135 (2018). <https://doi.org/10.1016/j.energy.2018.07.202>
27. Sahin, S., Cıgızoğlu, H.K.: The sub-climate regions and the sub-precipitation regime regions in turkey. *Journal of Hydrology* 180–189 (2012)
28. Toy, S., Kántor, N.: Evaluation of human thermal comfort ranges in urban climate of winter cities on the example of erzurum city. *Environ. Sci. Pollut. Res.* **24**(2), 1811–1820 (2017). <https://doi.org/10.1007/s11356-016-7902-8>
29. May, R., Arms, S., Leeman, J., Chastang, J.: Siphon: a collection of python utilities for accessing remote atmospheric and oceanic datasets. Unidata (2014–2017). <https://doi.org/10.5065/D6CN72NW> <https://github.com/Unidata/siphon>
30. May, R.M., Goebbert, K.H., Thielen, J.E., Leeman, J.R., Camron, M.D., Bruick, Z., Bruning, E.C., Manser, R.P., Arms, S.C., Marsh, P.T.: MetPy: a meteorological python library for data analysis and visualization. *Bull. Amer. Meteorol. Soc.* **103**(10), E2273–E2284 (2022). <https://doi.org/10.1175/BAMS-D-21-0125.1>, <https://journals.ametsoc.org/view/journals/bams/103/10/BAMSD-21-0125.1.xml>
31. Salby, M.L.: *Fundamentals of atmospheric physics* **61** (1996)
32. Li, J., Huang, H.-L.: Retrieval of atmospheric profiles from satellite sounder measurements by use of the discrepancy principle. *Appl. Opt.* **38**(6), 916–923 (1999). <https://doi.org/10.1364/AO.38.000916>
33. Li, J., Wolf, W.W., Menzel, W.P., Zhang, W., Huang, H.-L., Achtor, T.H.: Global soundings of the atmosphere from atovs measurements: the algorithm and validation. *J. Appl. Meteorol.* **39**(8), 1248–1268 (2000). [https://doi.org/10.1175/1520-0450\(2000\)039<1248:GSOTAF>2.0.CO;2](https://doi.org/10.1175/1520-0450(2000)039<1248:GSOTAF>2.0.CO;2)
34. Martinez, M.A.: Improvements in version 2013 of the nwcsaf/msg pge13 seviri physical retrieval (sphr) product. In: *The 2013 EUMETSAT Meteorological Satellite Data User's Conference*, Vienna, Austria (2013). <https://www.eumetsat.int/media/15708>
35. Özdemir, S., Yeşilyaprak, C., Aktuğ, B., Öztürk, D., Çoker, D., Balbay, R.: Precipitable water vapor (pww) estimations from the site of the eastern anatolia observatory (dag), a new astronomical observatory in turkey. *Exp. Astron.* **46**(2), 323–336 (2018). <https://doi.org/10.1007/s10686-018-9605-2>
36. Kidger, M.R., Rodriguez-Espinosa, J.M., del Rosario, J.C., Tranco, G.: Water vapour monitoring at the roque de los muchachos observatory (1996–1998). *New Astron. Rev.* **42**(6), 537–542 (1998). [https://doi.org/10.1016/S1387-6473\(98\)00068-2](https://doi.org/10.1016/S1387-6473(98)00068-2)

**Publisher's Note** Springer Nature remains neutral with regard to jurisdictional claims in published maps and institutional affiliations.

## Authors and Affiliations

Recep Balbay<sup>1,2</sup> · Kazım Kaba<sup>2</sup> · Süleyman Fişek<sup>3,4</sup> · Cahit Yeşilyaprak<sup>2,4</sup>

✉ Recep Balbay  
recep.balbay@tubitak.gov.tr

Kazım Kaba  
kazimkaba@atauni.edu.tr

Süleyman Fişek  
sfisek@istanbul.edu.tr

Cahit Yeşilyaprak  
cahity@atauni.edu.tr

<sup>1</sup> TÜBİTAK Space Technologies Research Institute (UZAY), Ankara 06800, Türkiye

<sup>2</sup> Faculty of Science, Department of Astronomy and Space Sciences, Atatürk University, Erzurum 25240, Türkiye

<sup>3</sup> Faculty of Science, Department of Astronomy and Space Sciences, İstanbul University, İstanbul 34119, Türkiye

<sup>4</sup> ATASAM-DAG, Türkiye National Observatories, Erzurum 25050, Türkiye